nature neuroscience

Calcium dynamics in astrocyte processes during neurovascular coupling

Yo Otsu[1,2,7], Kiri Couchman[1,2,7], Declan G Lyons[1,2], Mayeul Collot[3,4], Amit Agarwal[5], Jean-Maurice Mallet[3,4], Frank W Pfrieger[6], Dwight E Bergles[5] & Serge Charpak[1,2]

Enhanced neuronal activity in the brain triggers a local increase in blood flow, termed functional hyperemia, via several mechanisms, including calcium (Ca^{2+}) signaling in astrocytes. However, recent *in vivo* studies have questioned the role of astrocytes in functional hyperemia because of the slow and sparse dynamics of their somatic Ca^{2+} signals and the absence of glutamate metabotropic receptor 5 in adults. Here, we reexamined their role in neurovascular coupling by selectively expressing a genetically encoded Ca^{2+} sensor in astrocytes of the olfactory bulb. We show that in anesthetized mice, the physiological activation of olfactory sensory neuron (OSN) terminals reliably triggers Ca^{2+} increases in astrocyte processes but not in somata. These Ca^{2+} increases systematically precede the onset of functional hyperemia by 1–2 s, reestablishing astrocytes as potential regulators of neurovascular coupling.

Brain activity increases cerebral blood flow using a feed-forward mechanism that is independent of energy consumption. Enhanced release of glutamate from excitatory neurons is thought to induce vessel dilation through three potential signaling pathways (for reviews see refs. 1–3). The 'neuron to arteriole' hypothesis posits that a glutamate-evoked rise in intracellular Ca^{2+} concentration ($[Ca^{2+}]_i$) in postsynaptic dendrites triggers the release of vasodilators and potassium. The 'astrocyte to arteriole' hypothesis suggests that glutamatergic activation of metabotropic glutamate receptor 5 (mGluR5) in astrocytes triggers a rise in $[Ca^{2+}]_i$, leading to the release of arachidonic acid and vasoactive metabolites. Recently, a 'pericyte to capillary' hypothesis[4,5] has been proposed to occur at the level of first-order capillaries, involving a local prostaglandin E_2–mediated dilation that precedes arteriole dilation[6].

The contribution of each pathway to functional hyperemia remains unresolved, as large mechanistic differences have been reported across brain regions. These divergent findings may result from region- or synapse-specific characteristics, as well as methodological differences, such as the stimulus parameters, the type and level of anesthesia[7] or the pharmacological approach. In particular, the involvement of astrocytes has recently been called into question. Several studies have reported that Ca^{2+} transients evoked in astrocytes in response to neuronal activity are rare and delayed relative to the onset of functional hyperemia[8–11]. However, these studies monitored Ca^{2+} signals in astrocyte cell bodies rather than their processes, from which vasoactive compounds are presumably released[12]. There is considerable evidence, from experience using chemical[13,14] and genetically encoded[15,16] Ca^{2+} sensors, that Ca^{2+} signals in astrocytes are highly compartmentalized and that activity in discrete regions of their processes, termed microdomains, are often uncorrelated with events that occur in the soma. These results suggest that astrocyte Ca^{2+} dynamics may be more heterogeneous and complex than previously assumed[17–19] and that activity in microdomains could be subject to local independent modulation[20]. The role of astrocytic mGluR5 signaling in triggering functional hyperemia has also been challenged, as application of mGluR5-selective antagonists failed to affect functional hyperemia[21] and mGluR5 expression is strongly downregulated in adult mice[22]. In addition, functional hyperemia persists in IP_3R2-knockout mice[11,23], and IP_3R2 is required for metabotropic receptor–induced Ca^{2+} signaling in astrocytes[24].

The olfactory bulb glomerulus is a small neural network ideal for studying neurovascular coupling because of its accessibility, well-defined circuitry and ability to be activated by defined stimuli. Nevertheless, the respective roles of astrocytes and local neurons in controlling blood flow in this region are controversial[25–27]. In particular, the role of postsynaptic neurons has been difficult to assess because of the dense dendrodendritic synaptic connectivity[28], the expression of mGluR5 on juxtaglomerular (JG) cell dendrites[29,30] and the diversity of these cells[31]. The role of astrocytes also remains unresolved owing to the restriction of previous imaging studies to their somatic responses. Here, we revisited the role of Ca^{2+} signaling in astrocytes upon activation of olfactory sensory neuron (OSN) terminals in both acute slices and *in vivo*. Using acute slices from juvenile *Aldh1l1-eGFP* mice loaded with the Ca^{2+} indicator Rhod-2, we find that stimulation of OSNs evokes Ca^{2+} increases in astrocyte somata that involve mGluR5, have a high threshold and occur with

[1]Institut National de la Santé et de la Recherche Médicale (INSERM), U1128, Paris, France. [2]Laboratory of Neurophysiology and New Microscopies, Université Paris Descartes, Paris, France. [3]Centre National de la Recherche Scientifique (CNRS), UMR 7203, Paris, France. [4]Laboratory of Biomolecules, Université Pierre et Marie Curie, Paris, France. [5]The Solomon H. Snyder Department of Neuroscience, Johns Hopkins University School of Medicine, Baltimore, Maryland, USA. [6]CNRS UPR 3212, University of Strasbourg, Institute of Cellular and Integrative Neurosciences (INCI), Strasbourg, France. [7]These authors contributed equally to this work. Correspondence should be addressed to S.C. (serge.charpak@parisdescartes.fr).

Received 25 September; accepted 24 November; published online 22 December 2014; doi:10.1038/nn.3906

a delay of several seconds relative to those in neurons. To investigate Ca^{2+} signals in mature astrocytes, including in their fine processes, we used adult mice expressing the Ca^{2+} sensor protein GCaMP3 (ref. 20) under the conditional control of the connexin 30 promoter[32]. In acute slices from these mice, mGluR5 agonists failed to trigger astrocytic Ca^{2+} signals in either somata or processes, although astrocytes still responded robustly to ATP. *In vivo*, odorants systematically evoked Ca^{2+} increases in astrocytes that were restricted to their processes and preceded functional hyperemia by 1–2 s. The spatiotemporal dynamics of these Ca^{2+} signals reestablish astrocytes as potential regulators of neurovascular coupling.

RESULTS

Pharmacological activation of Ca^{2+} signals in astrocytes

We first analyzed the role of group I mGluRs (mGluR1 and mGluR5) in generating Ca^{2+} signals in neurons and astrocytes within the olfactory bulb glomerulus. In acute slices from juvenile (post-embryonic day 14 (P14)–P21) *Aldh1l1-eGFP* mice[33] incubated with the Ca^{2+} indicator Rhod2-AM (Rhod-2), astrocyte somata were co-labeled in red (Rhod-2) and green (eGFP), whereas neuron somata were red (Rhod-2). Because this approach did not allow us to distinguish neuronal from astrocytic processes, quantification of astrocyte Ca^{2+} dynamics was limited to somatic signals. Pressure application of the broad-spectrum mGluR agonist *trans*-1-aminocyclopentane-1,3-dicarboxylic acid (*t*-ACPD) reliably triggered transient Ca^{2+} increases in both astrocyte and neuron somata (**Fig. 1**), when AMPA/NMDA receptors, $GABA_A/GABA_B$ receptors and voltage-gated sodium channels were blocked (**Fig. 1a**,**b**). The specific mGluR5 antagonist 2-methyl-6-(phenylethynyl)pyridine (MPEP) strongly inhibited *t*-ACPD–evoked Ca^{2+} responses in astrocytes (**Fig. 1a**,**b**). In JG neurons, the degree of inhibition by MPEP was more variable (**Fig. 1b**), in accordance with the known variation in expression of various mGluR subtypes among these neurons[29,31]. The mGluR1 antagonist CPCCOEt strongly reduced *t*-ACPD–evoked Ca^{2+} responses in neurons but was less effective at inhibiting astrocyte responses (**Fig. 1c**,**d**). These results point to a prominent contribution of mGluR5 to *t*-ACPD–induced somatic Ca^{2+} responses in astrocytes in these juvenile mice. In contrast, the smaller effect of mGluR1 blockade on astrocytes raises the possibility that astrocytes may be responding to an indirect signal mediated by glomerular neurons (for example, dendritic glutamate release triggered by mGluR1 activation).

Synaptic activation of Ca^{2+} signals in astrocytes

As pressure application of *t*-ACPD indiscriminately activates synaptic and extrasynaptic mGluRs, we next investigated the physiological activation of mGluRs in response to glutamate release from OSN terminals. In acute slices from juvenile *Aldh1l1-eGFP* mice, single-pulse stimulation of OSN axons distant from their target glomerulus elicited prolonged Ca^{2+} responses in neuronal somata, but not in astrocytes (**Fig. 2**). In contrast, astrocyte somata responded only to higher stimulus intensities, and then with a 20-fold longer delay (4.5 ± 0.7 s; $n = 16$ cells, nine mice) than that of neurons (0.18 ± 0.02 s (mean ± s.e.m.); $n = 27$ cells, ten mice). This difference in stimulus threshold for astrocytes persisted when trains of stimuli were applied at 20 Hz: brief stimulus trains (0.5 s) evoked Ca^{2+} increases in JG neurons only, whereas longer trains (1–2 s) triggered delayed and slowly rising Ca^{2+} signals in astrocytes (**Supplementary Fig. 1a–c**). Notably, responsive astrocytes were observed in only 14% of all

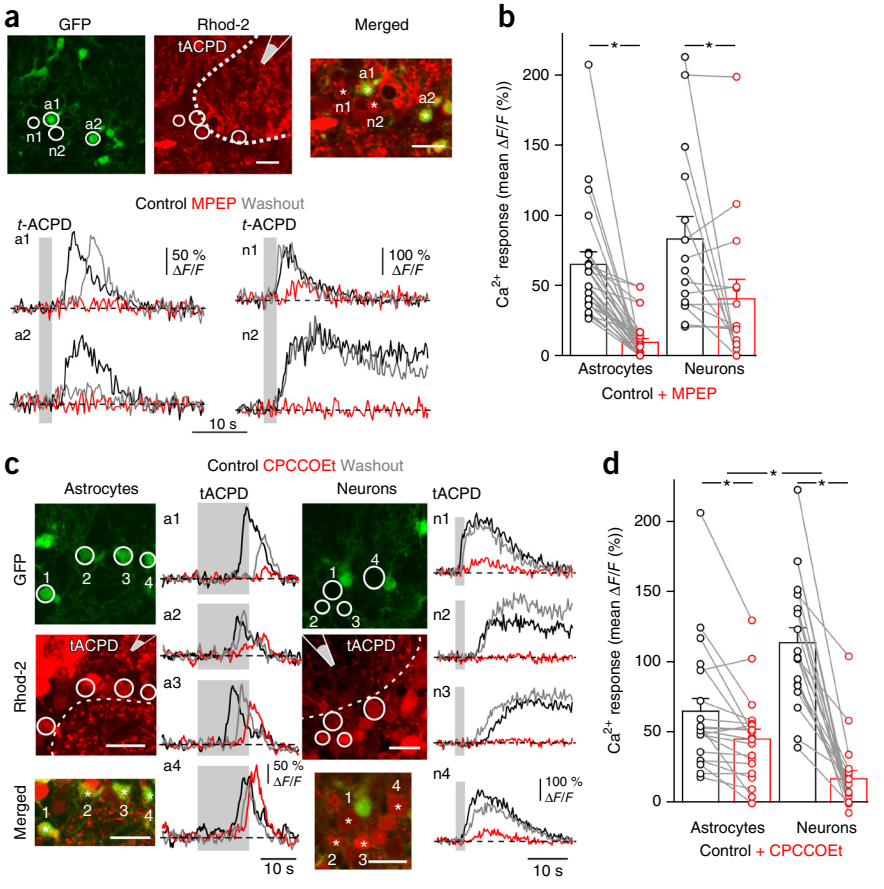

Figure 1 Somatic Ca^{2+} signals mediated by group 1 mGluRs in astrocytes and juxtaglomerular neurons of *Aldh1l1*-eGFP mice. (**a**) Top, Slices from juvenile mice, astrocytes (a1, a2) were co-labeled in red (Rhod-2) and green (GFP); neurons (n1, n2) are red. Puff pipette containing 0.5 mM *t*-ACPD was placed above slice surface. Dotted line indicates glomerular boundary. Merged, magnification of soma ROIs, asterisks mark recorded cells. Bottom, Ca^{2+} signals evoked by 2 s puff of *t*-ACPD (gray area) in control solution (black; solution contains 20–30 µM NBQX, 100 µM DAPV, 5–10 µM SR95531, 5–10 µM CGP55845A and 1 µM TTX), with the mGluR5 antagonist, MPEP (10 µM) (red) and after washout (gray). (**b**) Summary showing MPEP blocks *t*-ACPD responses in astrocytes ($P < 0.001$; $n = 22$ cells, 5 slices, 5 mice) and in some neurons ($P = 0.047$; $n = 15$ cells, 5 slices, 4 mice). (**c**) The mGluR1 antagonist CPCCOEt (100 µM) (red) had diverse effects on astrocytes (a1–a4) and neurons (n1–n4). Traces smoothed using a three-point sliding boxcar. (**d**) Summary showing CPCCOEt reduces responses in astrocytes ($P = 0.002$; $n = 20$ cells, 4 slices, 4 mice) and neurons ($P < 0.001$; $n = 19$ cells, 5 slices, 5 mice). The decrease in Ca^{2+} responses was lower for astrocytes (27.5 ± 7.0 $\Delta F/F$ %) than for neurons (83.4 ± 5.0 $\Delta F/F$ %) ($P < 0.001$). Data are mean ± s.e.m. Images are summed projections of control recordings. Scale bars, 20 µm. Lines in **b** and **d** connect data from individual cells (circles). Significance was assessed using a Wilcoxon signed-rank test.

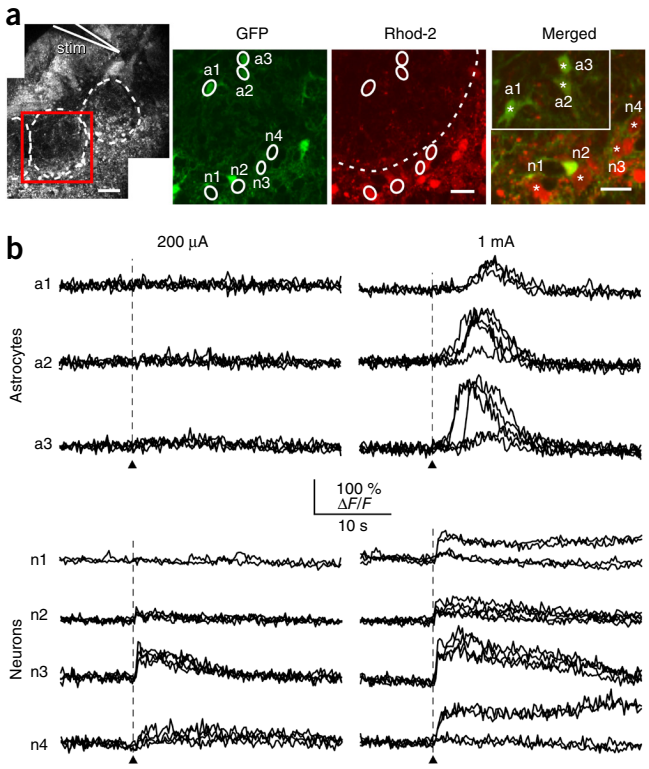

Figure 2 Synaptic activation of Ca^{2+} signals in glomerular astrocyte somata. (**a**) Left, for OSN stimulation, a theta pipette (stim) was placed into a bundle of OSN axons leading into a glomerulus (white dashed line). Scale bar, 50 µm. Red square indicates ROI used for recording within this glomerulus. Right, GFP and Rhod-2 fluorescence allowed for the identification of 7 cells of interest (white circles; astrocytes: a1–a3, neurons: n1–n4). Cell bodies are indicated by a star in the magnified merged image (astrocytes inset). All images are summed projections of images taken during the recording under control conditions (black traces); scale bars, 20 µm. Neuron ROIs were determined during activation. (**b**) From the cells shown in **a**, recordings of responses to a single OSN stimulation (arrowheads, 100-µs duration). Repetitions of trials with a stimulus intensity of 200 µA (left column) and 1 mA (right column) are superimposed. Experiment was repeated (n = 27 cells, 10 slices).

glomeruli stimulated with a single pulse (100 glomeruli in 79 slices from 62 animals), raising the possibility that stimulation of a single OSN axon bundle is insufficient to activate the entire glomerular volume and that glutamate spillover may be required to trigger somatic Ca^{2+} signals in astrocytes. Indeed, application of the glutamate transporter antagonist *threo*-β-benzyloxyaspartic acid (TBOA) or (trifluoromethyl)benzoylamino-TBOA (TFB-TBOA) decreased the threshold and increased the amplitude of Ca^{2+} transients in astrocyte somata induced by OSN stimulation (**Fig. 3a–c**). It also increased the percentage of glomeruli containing responsive astrocytes to 70% (ten glomeruli in ten slices from eight animals). However, these antagonists also caused a persistent increase in resting Ca^{2+} levels in all JG neurons (**Fig. 3d**), decreased their response to OSN stimulation and eventually induced Ca^{2+} oscillations (**Fig. 3b**), presumably by increasing ambient glutamate levels[34]. These results indicate that glutamate transporter inhibition causes substantial changes to the basal state of the glomerular neuronal network and is therefore unsuitable to investigate the input-output function of astrocytes.

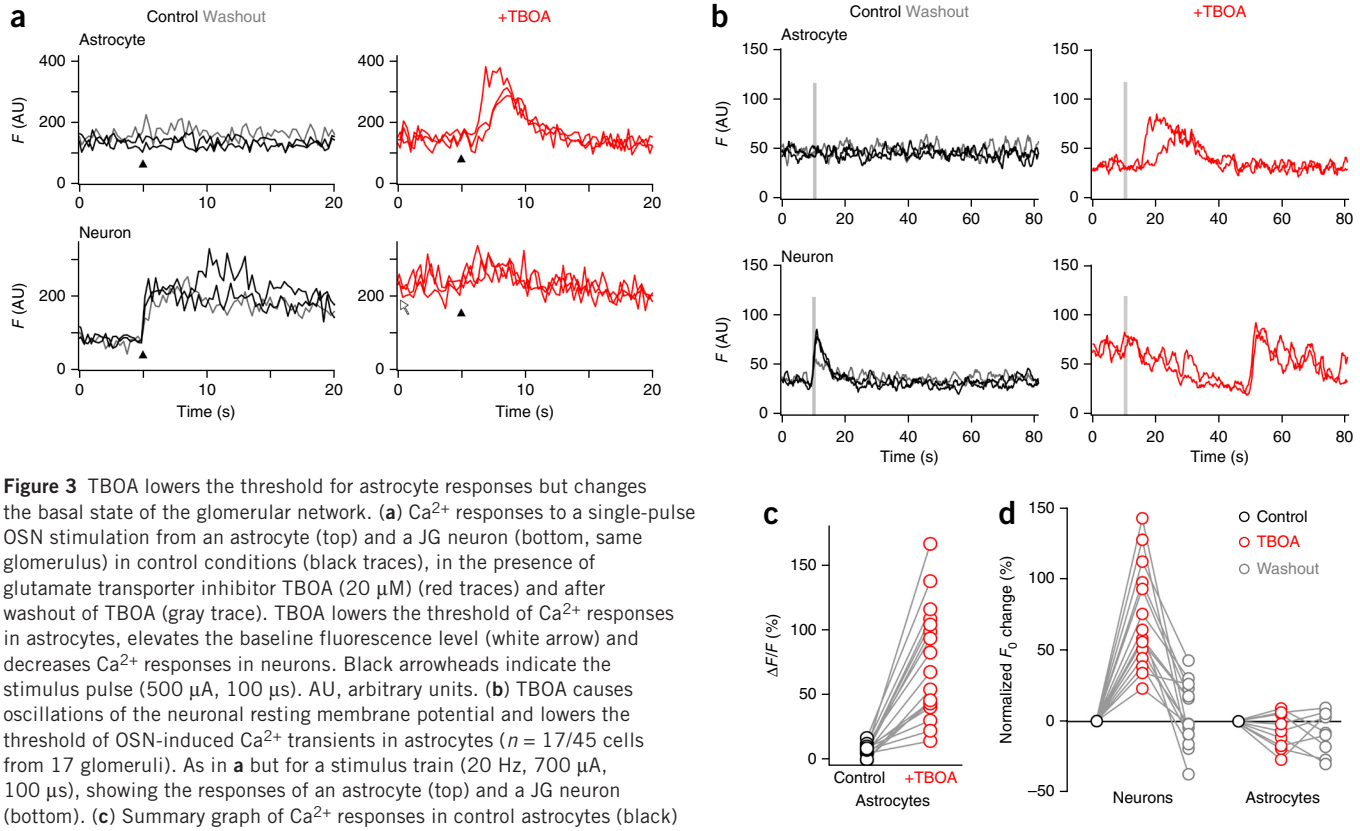

Figure 3 TBOA lowers the threshold for astrocyte responses but changes the basal state of the glomerular network. (**a**) Ca^{2+} responses to a single-pulse OSN stimulation from an astrocyte (top) and a JG neuron (bottom, same glomerulus) in control conditions (black traces), in the presence of glutamate transporter inhibitor TBOA (20 µM) (red traces) and after washout of TBOA (gray trace). TBOA lowers the threshold of Ca^{2+} responses in astrocytes, elevates the baseline fluorescence level (white arrow) and decreases Ca^{2+} responses in neurons. Black arrowheads indicate the stimulus pulse (500 µA, 100 µs). AU, arbitrary units. (**b**) TBOA causes oscillations of the neuronal resting membrane potential and lowers the threshold of OSN-induced Ca^{2+} transients in astrocytes (n = 17/45 cells from 17 glomeruli). As in **a** but for a stimulus train (20 Hz, 700 µA, 100 µs), showing the responses of an astrocyte (top) and a JG neuron (bottom). (**c**) Summary graph of Ca^{2+} responses in control astrocytes (black) and astrocytes in the presence of TBOA (red). (**d**) Summary graphs comparing the effect of TBOA (20–100 µM) on resting Ca^{2+} fluorescence in JG neurons (n = 15 cells, 5 slices, 5 mice) and astrocytes (n = 9 cells, 3 slices, 3 mice). Lines connect data from individual cells (open circles).

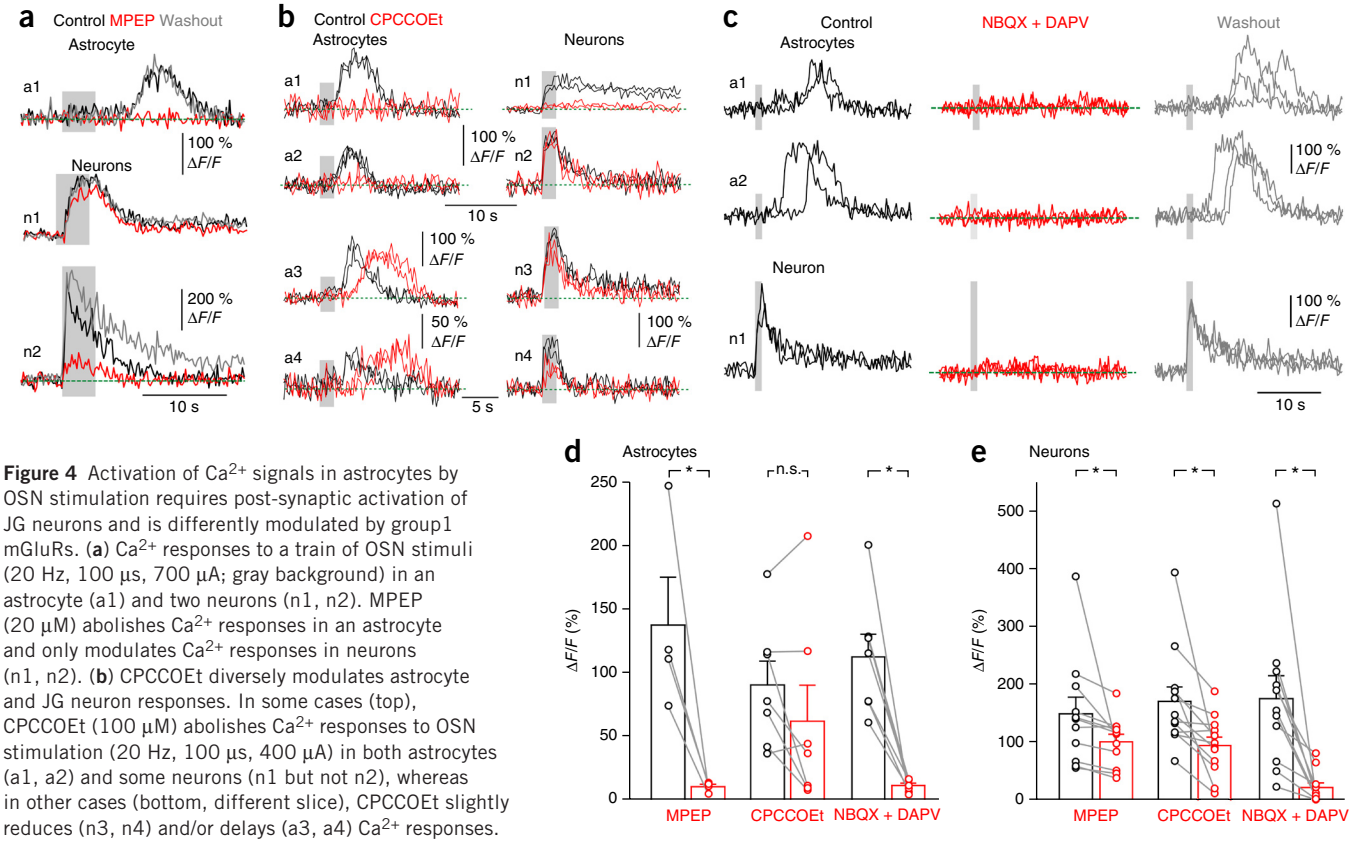

Figure 4 Activation of Ca^{2+} signals in astrocytes by OSN stimulation requires post-synaptic activation of JG neurons and is differently modulated by group1 mGluRs. (**a**) Ca^{2+} responses to a train of OSN stimuli (20 Hz, 100 µs, 700 µA; gray background) in an astrocyte (a1) and two neurons (n1, n2). MPEP (20 µM) abolishes Ca^{2+} responses in an astrocyte and only modulates Ca^{2+} responses in neurons (n1, n2). (**b**) CPCCOEt diversely modulates astrocyte and JG neuron responses. In some cases (top), CPCCOEt (100 µM) abolishes Ca^{2+} responses to OSN stimulation (20 Hz, 100 µs, 400 µA) in both astrocytes (a1, a2) and some neurons (n1 but not n2), whereas in other cases (bottom, different slice), CPCCOEt slightly reduces (n3, n4) and/or delays (a3, a4) Ca^{2+} responses. (**c**) AMPA and NMDAR antagonists (30 µM NBQX and 100 µM APV) (red) reversibly block Ca^{2+} responses in both cell types. Several traces are superimposed. (**d**) Left, summary graph showing the effects of MPEP (20 µM), CPCCOEt and NBQX (20–30 µM) + DAPV (100 µM), on somatic astrocytic Ca^{2+} responses elicited by OSN stimulation ($P = 0.042$ (Student's *t*-test), $P = 0.176$, $P = 0.018$). Right, summary graph showing the effects of MPEP, CPCCOEt and NBQX + DAPV on neuronal Ca^{2+} responses ($P = 0.004$, $P = 0.003$, $P = 0.003$). Lines connect data from individual cells (circles). Significance was assessed using a Wilcoxon signed-rank test, except where indicated. Data are presented as mean ± s.e.m.

We next tested the contribution of mGluRs to stimulation-induced Ca^{2+} responses in astrocytes and neurons. The mGluR5 antagonist MPEP markedly reduced stimulus-evoked Ca^{2+} responses in astrocyte somata (**Fig. 4a**) but did so less efficiently in neurons, similar to the effects observed for *t*-ACPD (**Fig. 1**). Blockade of mGluR1s with CPCCOEt had variable effects on Ca^{2+} signals evoked in both neurons and astrocytes (**Fig. 4b**). In JG cells, it ranged from no effect to a full blockade, and although on average there was a significant decrease (**Fig. 4e**), it is clear that not all neurons expressed mGluR1s. In astrocytes, Ca^{2+} signals were occasionally abolished (reversibly) or delayed, but on average the effect was not significant (**Fig. 4d**). Given the high stimulation threshold of somatic Ca^{2+} signals in astrocytes (**Fig. 2**) and assuming mGluR1 is not expressed by these cells[35], the modulatory effects of CPCCOEt suggest that astrocytes are indirectly activated by glutamate released from glomerular dendrites. Indeed, bath application of the AMPA and NMDA receptor antagonists 2,3-dihydroxy-6-nitro-7-sulfamoyl-benzo[f]quinoxaline-2,3-dione (NBQX) and D-2-amino-5-phosphonovalerate (DAPV) decreased or abolished Ca^{2+} responses evoked in both JG neurons (abolition in eight of eleven cells) and astrocytes (abolition in six of seven cells) by high-intensity stimulation of OSNs (**Fig. 4c**).

Together, these results suggest that generation of somatic Ca^{2+} signals in astrocytes in the juvenile mouse olfactory bulb requires activation of postsynaptic neurons, dendritic release of glutamate and activation of mGluR5 on astrocytes (see the schema in **Supplementary Fig. 2**), in accordance with the rarity and long latency of somatic Ca^{2+} signals observed *in vivo* upon sensory stimulation[8–11]. However, these studies are limited by the bulk-loading of AM dyes, which hinders selective imaging of astrocytic processes in adults *in vivo*, and by the relative immaturity of the mice used in our study (a requirement for efficient dye loading in the glomerulus). To overcome these limitations, we sought to visualize Ca^{2+} signals in the processes of glomerular astrocytes from adult mice using a genetically encoded Ca^{2+} sensor.

Cx30 promoter–driven expression of GCaMP3

To visualize Ca^{2+} transients in astrocytes, we expressed a cytosolic form of GCaMP3 (ref. 20) in astrocytes using the astrocyte-specific promoter connexin 30 (Cx30, also known as Gjb6). Cx30 is a gap-junction protein with a late postnatal onset of expression beginning in the second postnatal week and reaching a maximum at approximately 4 weeks after birth[32]. To target GCaMP3 to astrocytes, we crossed *Cx30-CreERT2* mice[36] to *R26-lsl-GCaMP3* mice[20]. To determine the cellular localization of GCaMP3, we performed immunohistochemical staining of sensor-expressing cells. In uninjected *Cx30-CreERT2*; *R26-lsl-GCaMP3* bitransgenic mice, sensor-expressing (GFP^+) cells were observed very rarely (glomerular layer: five astrocytes, zero neurons; granule cell/external plexiform layers: 10 astrocytes, 18 neurons; internal plexiform layer/rostral migratory stream: 4 astrocytes, 134 neurons; total of 24 slices, $n = 3$ mice). These results are probably due to slight tamoxifen-independent recombination in Cx30-expressing astrocytes and neuronal precursors[37].

When we administered 4-hydroxy-tamoxifen (4-OHT) to 2- to 3-month-old *Cx30-CreERT2*; *R26-lsl-GCaMP3* mice and analyzed

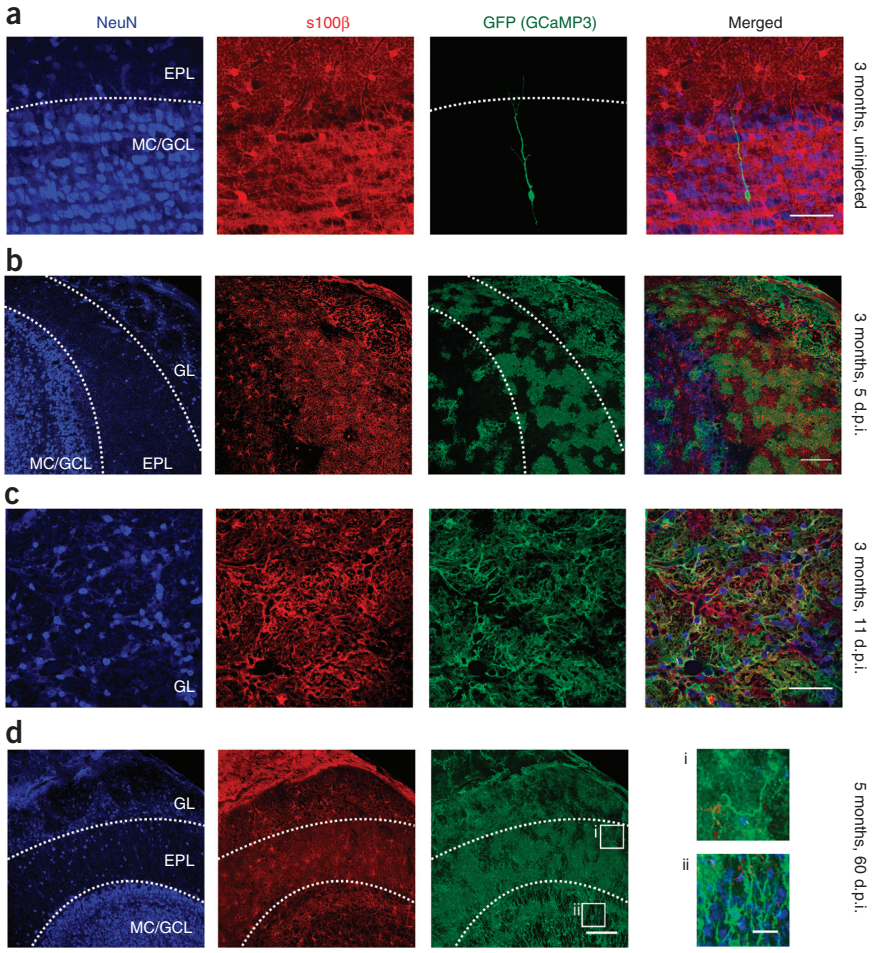

Figure 5 GCaMP3 expression in glomerular layer astrocytes of adult *Cx30-CreERT2*; *R26-lsl-GCaMP3* mice. (**a**) Horizontal section of olfactory bulb from a 3-month-old uninjected mouse labeled for neurons (NeuN), astrocytes (S100β) and GCaMP3 (GFP). One of the very few granule cells labeled, likely due to leak of $CreER^{T2}$. Dendrites are immature and terminate in the EPL. Scale bar, 50 µm. (**b**) GCaMP3 expression in a mouse at 5 d.p.i. (by 4-OHT injection); a large proportion of olfactory bulb astrocytes are labeled. No neurons were apparent in the glomerular layer ($n = 2$ mice). Scale bar, 100 µm. (**c**) Closer view of the glomerular layer in a mouse at 11 d.p.i.; all GCaMP3-labeled cells and processes are S100β positive, and there are no neurons or neuronal processes visible ($n = 2$ mice). Scale bar, 50 µm. (**d**) Section from a 5-month-old mouse at 2 months after the induction of GCaMP3 expression ($n = 2$ mice). Scale bar, 100 µm. A large number of neurons are now labeled in the granule cell layer (ii), and the dendritic segments are visible in the EPL (i). Far right, higher-magnification image of these neuron segments (i and ii), probably part of the population of newborn neurons. The *Cx30-CreERT2*; *R26-lsl-GCaMP3* mouse is no longer suitable for use in the imaging of astrocytic Ca^{2+} at this stage, so recordings were restricted to 5–11 d.p.i. Scale bars, 20 µm. GL, glomerular layer; EPL, external plexiform layer; MC/GCL, mitral cell/granule cell layer.

them 5–11 d post injection (d.p.i.), we observed GCaMP3 in a large fraction of olfactory bulb astrocytes, as shown by co-labeling with S100β (**Fig. 5a**). Notably, GCaMP3 was not expressed by neurons in the glomerular layer ($n = 4$ adult mice) (**Fig. 5b**,**c**). However, by 60 d.p.i. ($n = 2$ adult mice), a significant population of $GCaMP3^+$ neurons, predominantly granule cells[36], was apparent (**Fig. 5d**). This was expected, as granule cells in the olfactory bulb are continuously generated from Cx30-expressing radial glial cells in the subventricular zone[37]. As a consequence, only mice from between 5 and 11 d.p.i., in which GCaMP3 expression level remained moderate and restricted to astrocytes, were used for functional imaging.

Effects of ATP and mGluR5 agonists in adults

To assess whether astrocytes in adult mice express mGluR5, we focally applied the group 1 mGluR agonist (*S*)-3,5-dihydroxyphenylglycine (DHPG) to acute olfactory bulb slices prepared from 2- to 3-month-old *Cx30-CreERT2*; *R26-lsl-GCaMP3* mice ($n = 7$ glomeruli from four mice). In this preparation cell bodies are often visible in the apparent 'middle' of a glomerulus (for example, **Fig. 6a** regions of interest (ROIs) 2 and 3) if the imaging plane is near the surface of a glomerular boundary (i.e., it includes part of the juxtaglomerular region containing neuron and astrocyte cell bodies). In the presence of CPCCOEt to isolate mGluR5 responses, DHPG failed to elicit Ca^{2+} signals in astrocyte somata or their processes (**Fig. 6b**,**d**,**f**). The inclusion of Alexa 594 in the application solution confirmed the spread of DHPG across the imaging area.

As the visibility and viability of astrocytes in the adult slice preparation can be problematic, we ensured that astrocytes responded to stimulation by subsequent application of ATP, which reliably elicited robust Ca^{2+} increases in the somata and processes of glomerular astrocytes (**Fig. 6c**,**d**,**f**). Trials with spontaneous events (**Fig. 6e**) were excluded from the analysis presented in **Figure 6f**. Together, these results suggest that mGluR5 does not contribute to Ca^{2+} signaling in adult olfactory bulb astrocytes.

Ca^{2+} dynamics in astrocyte processes during odor stimulus

To determine if and when astrocytes are activated by physiological stimulation, we next simultaneously recorded the response of neurons and astrocytes to sensory input *in vivo* by measuring odor-evoked signals in the glomerulus of adult, anesthetized *Cx30-CreERT2*; *R26-lsl-GCaMP3* mice. Imaging of neuronal Ca^{2+} signals was accomplished by introduction of calcium Ruby nano dextran (CaRuby-Nano)[38], a high-affinity red Ca^{2+} indicator, into OSNs via nose labeling (Online Methods). Imaging was carried out in the superficial part of the glomerular layer (up to 70 µm from the olfactory bulb surface), and ROIs covered the entire center of the glomerulus, largely devoid of neuron and astrocyte cell bodies[39]. The glomerulus was delineated by labeled OSN terminals (red) and astrocyte processes (green). Ca^{2+} responses in OSN terminals provided a reliable readout of the onset and time course of odor-evoked postsynaptic neuronal responses and allowed for the alignment of normally imprecise respiration-linked response onsets for averaging[40]. At low temporal and spatial resolution (Online Methods and **Fig. 7** legend), odor-evoked OSN responses as reported by CaRuby-Nano were apparent, but GCaMP3 responses in astrocytes could not be detected (**Fig. 7a**). At higher resolution, small but consistent Ca^{2+} increases were detected in

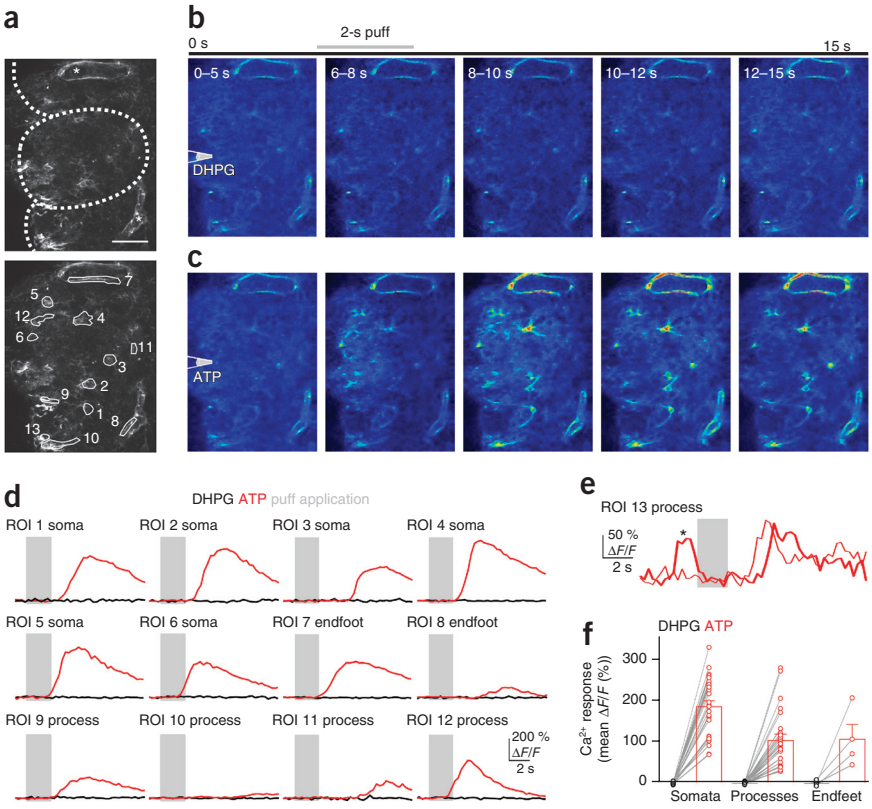

Figure 6 Effects of ATP and mGluR5 agonists on glomerular astrocytes from adult *Cx30-CreERT2*; *R26-lsl-GCaMP3* mice. (**a**) Top, a number of astrocytes are labeled, including endfeet processes (asterisks) outlining blood vessels. Dotted lines indicate glomerular boundaries. Bottom, ROIs covering astrocyte somata (1–6), endfeet (7 and 8) and processes (9–12). Images are maximum projections from around the imaging plane (i.e., the surface at 20 µm above to 10 µm below). Scale bar, 50 µm. (**b**) Averages of movie stills (taken at 3.3 Hz) taken during the indicated time intervals. Puff is triggered at 5 s for 2 s (gray bar) from pipette positioned above slice surface. Puffs of 100 µM DHPG (in the presence of 100 µM CPCCOEt) failed to elicit Ca^{2+} increases in astrocytes. (**c**) In the same glomerulus, subsequent puff application of 500 µM ATP elicits robust Ca^{2+} increases, indicating that astrocytes are viable. (**d**) Responses from ROIs shown in **a** to DHPG (black) and ATP (red). Gray bars indicate puff application. Responses are averages from 3–5 trials (trials with spontaneous activity were omitted from the average). (**e**) Example of two successive trials recorded from the astrocyte process in ROI 13. In one (thick trace), a rapid spontaneous event (asterisk) precedes the stimulus. Consequently, this ROI was not used for further analysis. (**f**) Average responses from all identified astrocyte somata, processes and endfeet to DHPG (black) and ATP (red) application (n = 27 somata, 26 processes, and 4 endfeet from 4 mice). Lines connect data from individual ROIs (circles). Data are presented as mean ± s.e.m.

astrocyte processes in all glomeruli tested (**Fig. 7b–d**). Ca^{2+} responses occurred reproducibly at the onset of each odor presentation with intertrial intervals of 3–4 min. The signal-to-noise ratio (SNR) of the responses and the frame rate (4–100 Hz) used to acquire Ca^{2+} signals did not allow us to resolve the delay between the neuronal and glial responses or to visualize Ca^{2+} transients within individual processes of astrocytes. In contrast, astrocyte somata that were occasionally visible at the periphery of the glomerulus (**Fig. 7c**) did not respond to the odor stimulus.

The short latency and reliability of odor-evoked responses in astrocyte processes suggest that astrocytic Ca^{2+} signals could play a role in neurovascular coupling. To determine the timing of odor-evoked astrocytic Ca^{2+} signals in relation to functional hyperemia, we imaged OSN terminals and Ca^{2+} transients within astrocyte processes while simultaneously monitoring red blood cell (RBC) velocity in glomerular capillaries of *Cx30-CreERT2*; *R26-lsl-GCaMP3* mice. To measure flow, we labeled blood plasma with Texas Red–labeled dextran and performed a broken line scan along the longitudinal axis of the capillary that extended into the glomerular neuropil, where Ca^{2+} signals in OSN terminals (labeled in red with CaRuby-Nano) and astrocyte processes (labeled in green with GCaMP3) could be measured. This approach allowed for simultaneous measurements of all three

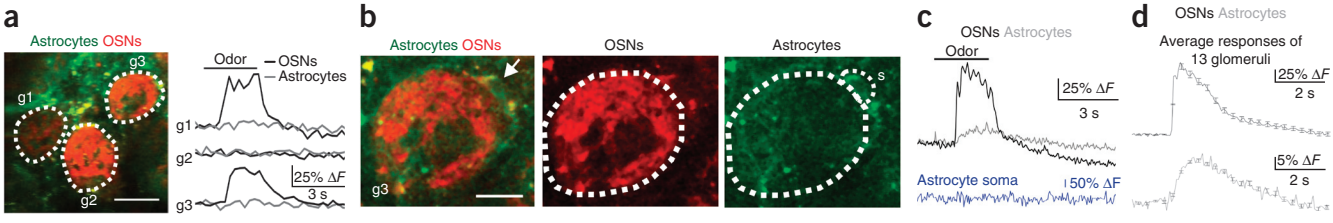

Figure 7 Astrocyte processes in *Cx30-CreERT2*; *R26-lsl-GCaMP3* mice reliably and rapidly respond to odor stimulation well before the onset of functional hyperemia. (**a**) Left, OSN terminals labeled with CaRuby-Nano (red) delineate glomerular boundaries (dotted lines; g1–g3), whereas GCaMP3 labeling at this stage (5–11 d.p.i.) is evident but weak and diffuse (green). Scale bar, 50 µm. Right, in response to odor stimulation (black bar), OSN inputs to two of the three glomeruli (g1 and g3) are activated (black traces), but it is difficult to resolve astrocyte responses (gray traces). Resolution: 1.1 µm per pixel, 271 ms per frame. (**b**) Average images from higher-resolution recordings of glomerulus g3. An astrocyte soma is visible at the periphery of the glomerulus (arrow). ROIs (dotted lines) outline OSNs terminating in the glomerulus (center, red) and astrocyte processes (right, green). Responses from the astrocyte soma are collected within the ROI labeled 's'. Scale bar, 20 µm. (**c**) Average of four trials showing the Ca^{2+} response of OSNs (black) and astrocytes (gray) to 3 s of odor stimulation with amyl acetate. The astrocyte soma (blue) does not respond. Resolution: 0.8 µm per pixel, 55 ms per frame. (**d**) Ensemble average of responses from all glomeruli (n = 13 glomeruli from 7 mice) showing the onset and duration of Ca^{2+} responses of OSNs (black) and astrocyte processes (gray). All traces were aligned by the onset of the OSN responses. Error bars show s.e.m.

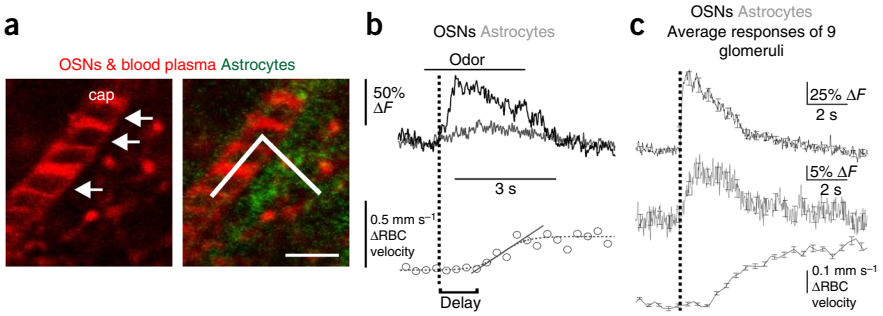

Figure 8 Astrocyte processes respond well before the onset of functional hyperemia. (**a**) Broken line scan acquisition was used to simultaneously measure RBC velocity in the capillary and record Ca^{2+} signals in both OSNs and astrocytes in the adjacent neuropil at a high temporal and spatial resolution. Left, Texas red–labeled dextran in the blood plasma labels a capillary lumen (cap), and RBCs are visible as shadows (arrows). Right, broken line scan (solid line) starts in the capillary to measure RBC velocity and is extended into the neuropil to collect Ca^{2+} responses from astrocyte processes (green) and OSN terminals (red). Scale bar, 5 µm. (**b**) Top, average (4 trials) of responses of OSNs (black) and astrocytes (gray) to odor stimulation with amyl acetate for 3 s. For clarity, the traces have been low-pass–filtered to 20 Hz. Bottom, simultaneous measurement of RBC velocity (circles) in the capillary shows an increase beginning ~1 s after the onset of the OSN response (vertical black dotted line). To determine this delay, the velocity data curve was fitted with a sigmoid (gray dotted line) and the onset of functional hyperemia estimated from the baseline intercept of a straight line fit to the rising phase of the response. (**c**) As in **b**, showing ensemble average of all glomeruli recorded (n = 9 glomeruli from 5 mice). Error bars show s.e.m.

responses at sampling rates of ~1 kHz, with a spatial resolution of 120–170 nm per pixel (**Fig. 8a**). As noted above, in every glomerulus where a Ca^{2+} response to odor occurred in OSNs, a Ca^{2+} increase was also observed in astrocytes (**Fig. 8b**). Under these conditions, odor stimuli also induced robust increases in RBC velocity, indicative of functional hyperemia. On average, changes in blood flow occurred 2.7 ± 0.23 s after the onset of OSN responses (**Fig. 8c**). Although it was not possible to precisely calculate the onset of astrocyte responses given the limited SNR achieved using the rapid-line-scan protocol, there is evidently only a short delay ($0 < t > 100$ ms) between OSN and astrocyte response onsets. To conclude, these *in vivo* findings indicate that odors induce Ca^{2+} transients in astrocyte processes within olfactory glomeruli several seconds before the onset of functional hyperemia, providing sufficient time for these cells to participate in local control of blood flow.

DISCUSSION

In this study, we show that neurons and astrocytes in the olfactory bulb of juvenile mice express different types of group 1 mGluRs, with astrocytes expressing primarily mGluR5 and neurons expressing varying amounts of mGluR5 and mGluR1. Although astrocytes in the adult OB no longer express mGluR5, they exhibit reliable calcium responses to odor stimulation *in vivo*, beginning seconds before the onset of functional hyperemia. Our results emphasize the importance of examining astrocyte processes, in addition to their somata, and reaffirm astrocytes as possible key players in neurovascular coupling. These findings help to resolve a controversy raised by several contradictory reports[25–27] investigating the role of astrocytes, mGluRs and postsynaptic neurons in neurovascular coupling in the olfactory bulb.

The unique synaptic organization of the glomerulus, notably the exceptional density of reciprocal dendrodendritic synaptic contacts, means that physiological activation of OSNs triggers a complex and prolonged cascade of synaptic activity. Consequently, pharmacological manipulation of postsynaptic activity is known to modulate the amount of both glutamate and GABA released upon OSN activation[40]. Gurden *et al.*[25] used intrinsic optical signals to monitor blood flow in glomeruli and reported that functional hyperemia is independent of both postsynaptic activity and mGluRs, instead involving glutamate transporters. However, a study from our laboratory[27] showed that pharmacological blockade of both glutamate receptors and glutamate release (with tetrodotoxin) within a single glomerulus does not block local neurovascular coupling, implying that the regulation of functional hyperemia occurs at a supraglomerular level. Furthermore, the widespread pharmacological blockade of postsynaptic glutamate receptors across the entire dorsal bulb abolished functional hyperemia, suggesting that activation of some postsynaptic components is required. Petzold *et al.*[26] reported that functional hyperemia involves glutamate transporters as well as mGluR5. However, the authors did not investigate the effect of a regional block of postsynaptic activity on functional hyperemia. Lastly, Sun *et al.*[22] reported that the expression of mGluR5 in astrocytes is developmentally downregulated to minimal levels after the third postnatal week, raising doubt as to the involvement of these receptors in neurovascular coupling. A previous study from the same group implicated mGluR5 in sensory-evoked astrocytic Ca^{2+} signals[8]; however, there was no direct evidence for their presence on astrocytes. Nonetheless, there is evidence for the expression of mGluR5 in olfactory bulb astrocytes from adult rat[35].

Our results indicate that in juvenile mice, mGluR5 is expressed by both JG neurons and astrocytes. This is in contrast to mGluR1, which probably influences astrocytes only indirectly via their presence on glomerular dendrites. We also show that, in contrast to neurons, somatic Ca^{2+} signals in astrocytes are only elicited by extremely strong activation of both OSNs and the postsynaptic glomerular network. We defined neurons as any eGFP-negative cells, although it may be argued that not all astrocytes are labeled in *Aldh1l1-eGFP* mice. Therefore, when stimulating with puff application of *t*-ACPD (**Fig. 1**), it is possible that some astrocytes may have been mistaken for neurons. However, in response to OSN stimulation (**Figs. 2–4**), the dynamics of the two cell populations defined in this manner were clearly different: GFP-negative 'neuronal' responses occurred at much shorter latencies and had faster rise times than those of eGFP-positive 'astrocytes', regardless of whether single stimuli or stimulus trains were used. Given the similarity of the conclusions from the two stimulus types, we are confident that neuron and astrocyte responses are well separated in our results. Our findings are congruent with several *in vivo* studies that have examined somatic Ca^{2+} signals in astrocytes, which concluded that their rarity and long latencies preclude them from having a role in neurovascular coupling[8–11]. However, these studies relied on bulk labeling with AM organic Ca^{2+} indicators to monitor astrocyte activity, which may not be suitable to monitor activity in fine astrocyte processes[41]. This is important, as recent studies suggest that Ca^{2+} transients in astrocytic processes are more frequent and often occur independently from somatic signals[26,41,42]. In our experiments using Rhod-2 AM, we found that neuropil responses had a much lower threshold than those from astrocyte somata (data not shown). It is likely that, in addition to OSN terminals and neuron

dendrites, astrocyte processes contributed to these signals but were not resolvable using bulk labeling. Indeed, in juvenile mice, astrocyte processes are sensitive to single synaptic stimulation[13], and in adults processes respond to spontaneous neuronal activity[14].

We find that the inhibition of glutamate transporters enhances stimulus-evoked Ca^{2+} signals in juvenile astrocyte somata. However, in neurons it also causes a rise in the resting Ca^{2+} level and a decrease in evoked Ca^{2+} signals. Consequently, if functional hyperemia depended only on astrocyte somatic Ca^{2+} signals evoked by glutamate release from OSN terminals and activation of astrocyte mGluR5, one would expect glutamate transporter antagonists to enhance functional hyperemia, but in fact the opposite effect has been reported[25,26]. Unfortunately, these antagonists induce a rise in extracellular glutamate that leads to sustained activation of glomerular neurons and astrocytes, precluding its use in studying the role of this pathway in functional hyperemia.

In vivo studies using another Ca^{2+} indicator dye, Oregon Green BAPTA 1-AM, reported fast synaptically evoked Ca^{2+} signals in somata[42,43] and processes[43] of cortical astrocytes. However, the latter study could not ensure separation of signals from labeled astrocyte processes, axonal terminals and thin dendrites. This issue could be solved by investigating the dynamics of Ca^{2+} in astrocyte processes that express genetically encoded Ca^{2+} sensors. However, expression of these genes relies on the use of astrocyte promoters, which are also active in glial progenitor cells. Ongoing adult neurogenesis represents a particular challenge for genetic labeling of astrocytes in the OB, as adult-born neurons are continually generated from these precursors[44,45]. This problem is well demonstrated by the considerable neuronal labeling apparent in *GLAST-ERT2*; *R26-lsl-GCaMP3* mice, which is probably a consequence of the early expression of GLAST in glial precursor cells[46]. To circumvent this problem, we used the postnatally active Cx30 promoter and a tamoxifen-dependent version of Cre recombinase to achieve GCaMP3 expression in astrocytes of adult mice[32,36]. We observed neuronal expression of GCaMP3 some weeks (~3 weeks) after induction, in accordance with previous observations that Cx30-positive radial glia generate neuroblasts. Nevertheless, astrocyte Ca^{2+} dynamics can be visualized selectively in both acute slices and *in vivo* if imaging is performed shortly after induction of Cre activity in *Cx30-CreERT2*; *R26-lsl-GCaMP3* mice.

We observed that in slices from adult *Cx30-CreERT2*; *R26-lsl-GCaMP3* mice, application of mGluR5s agonists failed to induce an elevation of astrocytic Ca^{2+}. One possibility is that we missed fast calcium elevation; however, the spatiotemporal resolution of our full-frame slice recordings (4 Hz) was sufficient to record spontaneous events restricted to astrocyte processes (**Fig. 6e**). This corroborates evidence that expression of mGluR5 is markedly downregulated in adult astrocytes[22], that functional hyperemia is maintained in IP_3R2-knockout mice[23,47,48] and that basal cortical blood flow is insensitive to selective stimulation of astrocytic Gq-GPCR cascades using the hM3Dq DREADD designer receptor system[48]. Moreover, our results indicate that if mGluR5s are expressed by neurons in adults, their influence is insufficient to trigger astrocytic activation indirectly. Importantly, our *in vivo* imaging revealed that astrocyte processes, but not their somata, reliably respond to sensory stimulation with a rapid onset that is nearly coincident with that of surrounding neurons. Further, the activation of both OSN terminals and astrocyte processes clearly precedes functional hyperemia by ~1–3 s. Unfortunately, the SNR of our current approach is too low to reliably quantify the relative onset of Ca^{2+} signals in OSNs and astrocyte processes. The use of animals expressing Ca^{2+} reporter proteins with a better SNR (for example, GCaMP6) or targeted to the membrane[16] may help to reveal the kinetics of responses in these small compartments. Taken together, our results emphasize the importance of imaging the fine processes of astrocytes, as they may more faithfully report synaptic activity, as shown *in vitro*[13,14]. We thus demonstrate that astrocytes respond to sensory stimulation with sufficient speed to allow them to play a role in neurovascular coupling. As a result, simultaneous investigation of astrocytes and pericytes[5], in anesthetized and awake mice, becomes the next challenge to determine the respective roles of these two cell types in the development and regulation of neurovascular coupling and resting vessel tone.

METHODS

Methods and any associated references are available in the online version of the paper.

Note: Any Supplementary Information and Source Data files are available in the online version of the paper.

ACKNOWLEDGMENTS

We would like to thank C. Pouzat for his critical comments. Support was provided by INSERM, the Agence Nationale de la Recherche (Project Angioneurins R11036KK), the Leducq Foundation, the Human Frontier Science Program Organization (RGP008912009-C), the Fondation pour la Recherche Médicale (equipe FRM) and the US National Institutes of Health (MH084020 to D.E.B.). K.C. was supported by the Agence Nationale de la Recherche and the ERC Advanced Grant "Imaging-in-the-magnet." D.G.L. was supported by a doctoral fellowship from École des Neurosciences de Paris (Paris School of Neuroscience) and a bursary from the Fondation pour la Recherche Médicale (FDT20130928252). The team of S.C. is part of the École des Neurosciences de Paris Ile-de-France network. We thank W. Fröstle (Ciba-Geigy) for the kind gift of CGP55845A (3-[1-(*S*)-(3,4-dichlorophenyl)ethyl]amino-2(*S*)hydroxypropyl-*P*-benzyl-phosphonic acid).

AUTHOR CONTRIBUTIONS

Y.O., K.C. and D.G.L. conducted the experiments, M.C. synthesized CaRuby-Nano, Y.O., K.C. and S.C. analyzed the data, Y.O., K.C., S.C. and J.-M.M. designed the research, A.A. and D.E.B. provided the *R26-lsl-GCaMP3* mouse line, and F.W.P. provided the *Cx30-CreERT2* mouse line. All authors edited the paper.

COMPETING FINANCIAL INTERESTS

The authors declare no competing financial interests.

1. Iadecola, C. & Nedergaard, M. Glial regulation of the cerebral microvasculature. *Nat. Neurosci.* **10**, 1369–1376 (2007).
2. Attwell, D., Buchan, A. & Charpak, S. Glial and neuronal control of brain blood flow. *Nature* **468**, 232–243 (2010).
3. Dunn, K.M. & Nelson, M.T. Neurovascular signaling in the brain and the pathological consequences of hypertension. *Am. J. Physiol. Heart Circ. Physiol.* **306**, H1–H14 (2014).
4. Peppiatt, C.M., Howarth, C., Mobbs, P. & Attwell, D. Bidirectional control of CNS capillary diameter by pericytes. *Nature* **443**, 700–704 (2006).
5. Bell, R.D. *et al.* Pericytes control key neurovascular functions and neuronal phenotype in the adult brain and during brain aging. *Neuron* **68**, 409–427 (2010).
6. Hall, C.N. *et al.* Capillary pericytes regulate cerebral blood flow in health and disease. *Nature* **508**, 55–60 (2014).
7. Masamoto, K. & Kanno, I. Anesthesia and the quantitative evaluation of neurovascular coupling. *J. Cereb. Blood Flow Metab.* **32**, 1233–1247 (2012).
8. Wang, X. *et al.* Astrocytic Ca^{2+} signaling evoked by sensory stimulation *in vivo*. *Nat. Neurosci.* **9**, 816–823 (2006).
9. Schummers, J., Yu, H. & Sur, M. Tuned responses of astrocytes and their influence on hemodynamic signals in the visual cortex. *Science* **320**, 1638–1643 (2008).
10. Schulz, K. *et al.* Simultaneous BOLD fMRI and fiber-optic calcium recording in rat neocortex. *Nat. Methods* **9**, 597–602 (2012).
11. Nizar, K. *et al. In vivo* stimulus-induced vasodilation occurs without IP3 receptor activation and may precede astrocytic calcium increase. *J. Neurosci.* **33**, 8411–8422 (2013).
12. Mulligan, S.J. & MacVicar, B.A. Calcium transients in astrocyte endfeet cause cerebrovascular constrictions. *Nature* **431**, 195–199 (2004).
13. Panatier, A. *et al.* Astrocytes are endogenous regulators of basal transmission at central synapses. *Cell* **146**, 785–798 (2011).
14. Di Castro, M.A. *et al.* Local Ca^{2+} detection and modulation of synaptic release by astrocytes. *Nat. Neurosci.* **14**, 1276–1284 (2011).

15. Shigetomi, E. & Kracun, S. A genetically targeted optical sensor to monitor calcium signals in astrocyte processes. *Nat. Neurosci.* **13**, 759–766 (2010).
16. Shigetomi, E. *et al.* Imaging calcium microdomains within entire astrocyte territories and endfeet with GCaMPs expressed using adeno-associated viruses. *J. Gen. Physiol.* **141**, 633–647 (2013).
17. Volterra, A., Liaudet, N. & Savtchouk, I. Astrocyte Ca^{2+} signalling: an unexpected complexity. *Nat. Rev. Neurosci.* **15**, 327–335 (2014).
18. Haustein, M.D. *et al.* Conditions and constraints for astrocyte calcium signaling in the hippocampal mossy fiber pathway. *Neuron* **82**, 413–429 (2014).
19. Rusakov, D.A.a, Bard, L., Stewart, M.G. & Henneberger, C. Diversity of astroglial functions alludes to subcellular specialisation. *Trends Neurosci.* **37**, 228–242 (2014).
20. Paukert, M. *et al.* Norepinephrine controls astroglial responsiveness to local circuit activity. *Neuron* **82**, 1263–1270 (2014).
21. Calcinaghi, N. *et al.* Metabotropic glutamate receptor mGluR5 is not involved in the early hemodynamic response. *J. Cereb. Blood Flow Metab.* **31**, e1–e10 (2011).
22. Sun, W. *et al.* Glutamate-dependent neuroglial calcium signaling differs between young and adult brain. *Science (80-.).* **339**, 197–200 (2013).
23. Jego, P., Pacheco-Torres, J., Araque, A. & Canals, S. Functional MRI in mice lacking IP_3-dependent calcium signaling in astrocytes. *J. Cereb. Blood Flow Metab.* **34**, 1599–1603 (2014).
24. Fiacco, T.A. *et al.* Selective stimulation of astrocyte calcium in situ does not affect neuronal excitatory synaptic activity. *Neuron* **54**, 611–626 (2007).
25. Gurden, H., Uchida, N. & Mainen, Z.F. Sensory-evoked intrinsic optical signals in the olfactory bulb are coupled to glutamate release and uptake. *Neuron* **52**, 335–345 (2006).
26. Petzold, G.C., Albeanu, D.F., Sato, T.F. & Murthy, V.N. Coupling of neural activity to blood flow in olfactory glomeruli is mediated by astrocytic pathways. *Neuron* **58**, 897–910 (2008).
27. Chaigneau, E. *et al.* The relationship between blood flow and neuronal activity in the rodent olfactory bulb. *J. Neurosci.* **27**, 6452–6460 (2007).
28. Shepherd, G.M., Chen, W.R. & Greer, C.A. in *The Synaptic Organization of the Brain* (ed. Shepherd, G.M.) 165–216 (Oxford University Press, 2004).
29. Dong, H.-W., Hayar, A. & Ennis, M. Activation of group I metabotropic glutamate receptors on main olfactory bulb granule cells and periglomerular cells enhances synaptic inhibition of mitral cells. *J. Neurosci.* **27**, 5654–5663 (2007).
30. Jian, K., Cifelli, P., Pignatelli, A., Frigato, E. & Belluzzi, O. Metabotropic glutamate receptors 1 and 5 differentially regulate bulbar dopaminergic cell function. *Brain Res.* **1354**, 47–63 (2010).
31. Kosaka, T. & Kosaka, K. "Interneurons" in the olfactory bulb revisited. *Neurosci. Res.* **69**, 93–99 (2011).
32. Kunzelmann, P. *et al.* Late onset and increasing expression of the gap junction protein connexin30 in adult murine brain and long-term cultured astrocytes. *Glia* **25**, 111–119 (1999).
33. Yang, Y. *et al.* Molecular comparison of $GLT1^+$ and $ALDH1L1^+$ astrocytes *in vivo* in astroglial reporter mice. *Glia* **59**, 200–207 (2011).
34. Jabaudon, D. *et al.* Inhibition of uptake unmasks rapid extracellular turnover of glutamate of nonvesicular origin. *Proc. Natl. Acad. Sci. USA* **96**, 8733–8738 (1999).
35. Van den Pol, A.N. Presynaptic metabotropic glutamate receptors in adult and developing neurons: autoexcitation in the olfactory bulb. *J. Comp. Neurol.* **359**, 253–271 (1995).
36. Slezak, M. *et al.* Transgenic mice for conditional gene manipulation in astroglial cells. *Glia* **55**, 1565–1576 (2007).
37. Bonfanti, L. & Peretto, P. Radial glial origin of the adult neural stem cells in the subventricular zone. *Prog. Neurobiol.* **83**, 24–36 (2007).
38. Oheim, M. *et al.* New red-fluorescent calcium indicators for optogenetics, photoactivation and multi-color imaging. *Biochim. Biophys. Acta* **1843**, 2284–2306 (2014).
39. Roux, L., Benchenane, K., Rothstein, J.D., Bonvento, G. & Giaume, C. Plasticity of astroglial networks in olfactory glomeruli. *Proc. Natl. Acad. Sci. USA* **108**, 18442–18446 (2011).
40. Lecoq, J., Tiret, P. & Charpak, S. Peripheral adaptation codes for high odor concentration in glomeruli. *J. Neurosci.* **29**, 3067–3072 (2009).
41. Reeves, A.M.B., Shigetomi, E. & Khakh, B.S. Bulk loading of calcium indicator dyes to study astrocyte physiology: key limitations and improvements using morphological maps. *J. Neurosci.* **31**, 9353–9358 (2011).
42. Winship, I.R., Plaa, N. & Murphy, T.H. Rapid astrocyte calcium signals correlate with neuronal activity and onset of the hemodynamic response *in vivo*. *J. Neurosci.* **27**, 6268–6272 (2007).
43. Lind, B.L., Brazhe, R., Jessen, S.B., Tan, F.C.C. & Lauritzen, M.J. Rapid stimulus-evoked astrocyte Ca^{2+} elevations and hemodynamic responses in mouse somatosensory cortex *in vivo*. *Proc. Natl. Acad. Sci. USA* **110**, E4678–E4687 (2013).
44. Winpenny, E. *et al.* Sequential generation of olfactory bulb glutamatergic neurons by Neurog2-expressing precursor cells. *Neural Dev.* **6**, 12 (2011).
45. Nissant, A. & Pallotto, M. Integration and maturation of newborn neurons in the adult olfactory bulb–from synapses to function. *Eur. J. Neurosci.* **33**, 1069–1077 (2011).
46. Hartfuss, E., Galli, R., Heins, N. & Götz, M. Characterization of CNS precursor subtypes and radial glia. *Dev. Biol.* **229**, 15–30 (2001).
47. Takata, N. *et al.* Cerebral blood flow modulation by basal forebrain or whisker stimulation can occur independently of large cytosolic Ca^{2+} signaling in astrocytes. *PLoS ONE* **8**, e66525 (2013).
48. Bonder, D.E. & McCarthy, K.D. Astrocytic Gq-GPCR-linked IP3R-dependent Ca^{2+} signaling does not mediate neurovascular coupling in mouse visual cortex *in vivo*. *J. Neurosci.* **34**, 13139–13150 (2014).

ONLINE METHODS

Transgenic mouse lines. Experimental protocols followed the INSERM health guidelines and have been approved by the University Paris Descartes Ethics Committee. Mice of both sexes were used. Mice expressing the enhanced green fluorescent protein (eGFP) under the control of the aldehyde dehydrogenase 1 family, member L1 (*Aldh1l1*) promoter were used for the experiments in acute slices using Rhod-2 labeling[33]. These mice were backcrossed onto an NMR1 background. For acute slices and *in vivo* imaging and immunohistochemical staining in adult mice, *Cx30-CreERT2*$^{+/-}$ (ref. 36) mice were crossed with *R26-lsl-GCaMP3*$^{+/+}$ (ref. 20) mice to target GCaMP3 expression to astrocytes. CreERT2 recombinase–mediated induction of GCaMP3 expression was induced by a single intraperitoneal injection of 2 mg 4-hydroxytamoxifen (Santa Cruz, sc-3542). *GLAST-CreERT*$^{+/-}$ mice (B6.Cg-Tg(Slc1a3-cre/ERT)1Nat/J, Jackson Labs) were also crossed with the *R26-lsl-GCaMP3*$^{+/+}$ line, and slices were processed for immunohistochemistry. These mice were initially tested for specific expression of GCaMP3 in astrocytes but could not be used because of strong neuronal expression, even in the absence of 4-OHT injection (see **Supplementary Fig. 3**). This was due to continuous activity of the GLAST promoter in neuronal precursors during development and in the adult and tamoxifen-independent background activity of CreERT2.

Slice preparation. Horizontal olfactory bulb slices (300 µm thick) were prepared from 14- to 21-day-old *Aldh1l1-eGFP* or 2- to 3-month-old *Cx30-CreERT2*; *R26-lsl-GCaMP3* mice. For juvenile mice, slices were cut in ice-cold oxygenated (5% CO_2 and 95% O_2) artificial cerebrospinal fluid (aCSF) containing (in mM) 110 choline-Cl, 25 $NaHCO_3$, 25 D-glucose, 11.6 L-ascorbic acid, 7 $MgSO_4$, 3.1 Na-pyruvate, 2.5 KCl, 1.25 NaH_2PO_4, 0.5 $CaCl_2$. Slices from adult mice were collected in oxygenated aCSF at room temperature (24 °C) containing (in mM) 83 NaCl, 26.2 $NaHCO_3$, 1 NaH_2PO_4, 2.5 KCl, 3.3 $MgSO_4$, 0.5 $CaCl_2$, 70 sucrose and 22 D-glucose. All slices were transferred to a recording solution containing (in mM) 125 NaCl, 25 $NaHCO_3$, 11 D-glucose, 2.5 KCl, 2 Na-pyruvate, 2 $CaCl_2$, 1 $MgCl_2$, and 0.4 l-ascorbic acid, for incubation (34 °C for 30 min) and then cooled to room temperature before recording.

Imaging in acute slices. *Juvenile Aldh1l1-eGFP mice.* Astrocytes and juxtaglomerular neurons were loaded with the Ca^{2+} indicator Rhod-2 AM (10 µM, Invitrogen) at room temperature (~25 °C) for 1 h with 0.02% Pluronic F-127 (Invitrogen) and 0.6% DMSO (Sigma) in aCSF. Bundles of OSN axons were stimulated using a theta pipette filled with aCSF. The electrical stimulus (100 µs) was delivered using an Isolator-11 Stimulus Isolator Unit (Molecular Devices). Glomeruli activated by OSN stimulation were identified by increased fluorescence in the dense neuropil at the center of the glomerulus. Ca^{2+} responses in astrocytes were defined as stimulus-evoked if they occurred with a latency of <5 s after the stimulus and in more than two trials. If spontaneous Ca^{2+} increases were detected within 10 s before the stimulus, the trace was excluded from analysis. For *in vitro* pharmacology, only those experiments where the responses could be partially recovered after drug washout were included.

For pressure-application, (±)-1-aminocyclopentane-*trans*-1,3-dicarboxylic acid (*t*-ACPD; 500 µM) (*S*)-3,5-dihydroxyphenylglycine (DHPG; 100 µM) or adenosine 5′-triphosphate disodium salt hydrate (ATP; 500 µM) were dissolved in aCSF and loaded into a glass pipette (tip resistance 2–3 MΩ) placed 20–40 µm above the slice. To image the spread of DHPG and ATP in adult slices after a puff, 10 µM Alexa Fluor 594 Hydrazide (Life Technologies) was included in the solution.

Fluorescence was imaged using a 63× water-immersion objective (Leica) with a custom-built two-photon laser scanning microscope. GFP and the Rhod-2 fluorophore were excited at 840 nm, and epifluorescence was detected with 500-nm (40 nm bandpass) and 620-nm (60 nm bandpass) filters (Chroma). GCaMP3 and Alexa Fluor 594 fluorophore were excited at 900–920 nm to reduce autofluorescence, and epifluorescence was detected with a 570-nm shortpass filter and a 620 (40 nm wide) bandpass filter (Chroma). Images were acquired in frame mode (250–350 ms per frame) with custom-made software (LabVIEW, National Instruments).

Drug application. *t*-ACPD, DHPG and ATP (Sigma) were applied by pressure-application through a patch pipette. Other agonists and blockers were applied through the bath perfusion. *t*-ACPD, 2-methyl-6-(phenylethynyl)pyridine hydrochloride (MPEP); 2,3-dioxo-6-nitro-1,2,3,4-tetrahydrobenzo[*f*]quinoxaline -7-sulfonamide (NBQX); D-(−)-2-amino-5-phosphonopentanoic acid (D-APV), 6-imino-3-(4-methoxyphenyl)-1(6*H*)-pyridazinebutanoic acid hydrobromide (SR95531), 7-(hydroxyimino)cyclopropa[*b*]chromen-1a-carboxylate ethyl ester (CPCCOEt), tetrodotoxin (TTX), DL-*threo*-β-benzyloxyaspartic acid (TBOA), (3*S*)-3-[[3-[[4-(trifluoromethyl)benzoyl]amino]phenyl]methoxy]-L-aspartic acid (TFB-TBOA), (*S*)-3,5-dihydroxyphenylglycine (DHPG) were purchased from Tocris or Abcam. We thank W. Fröstle for the kind gift of CGP55845A (3-[1-(*S*)-(3,4-dichlorophenyl)ethyl]amino-2(*S*)hydroxypropyl-*P*-benzyl-phosphonic acid).

Immunohistochemistry. *Cx30-CreERT2*; *R26-lsl-GCaMP3* and *GLAST-CreERT2*; *R26-lsl-GCaMP3* mice were perfused transcardially with PBS followed by 4% paraformaldehyde (PFA). After post-fixation overnight in 4% PFA, 50-µm sections were cut using a vibrating microtome. Slices were incubated in blocking solution for 1 h (PBS containing 2% BSA and 0.1% Triton X-100) and then with primary antibodies against GFP (chicken IgY antibody fraction: Invitrogen A10262, 1:1,000) S100β (rabbit polyclonal: Abcam Z0311, 1:500) and NeuN (mouse monoclonal (clone A60): Millipore MAB377, 1:500) at 4 °C overnight. After washing, slices were incubated with secondary antibodies (1:500; Alexa Fluor 488 goat anti-chicken IgG (1:500; Invitrogen A11039), Alexa Fluor 546 goat anti-mouse IgG (H+L) (1:500; Invitrogen A11030), Alexa Fluor 633 goat anti-mouse IgG (H+L) (1:500; Invitrogen A21050)) for 2 h at room temperature, then rinsed in PBS and mounted in Vectashield (Vector Laboratories) for confocal microscopy (Zeiss LSM-510). Images were prepared in ImageJ (NIH). All images presented are SD projections of image stacks with a linear correction of brightness and contrast.

Nose-loading of Calcium Ruby Nano. 2- to 3-month-old mice were anesthetized by intraperitoneal injection of ketamine (100 mg kg^{-1}) and xylazine (8 mg kg^{-1}) in 0.9% NaCl, and laid on their backs where they remained until they recovered from anesthesia. 8–10 µl of a solution containing 4 mM Calcium Ruby Nano (CaRuby-Nano) dextran (6 kDa), 2% Triton X-100 (Sigma-Aldrich) in PBS was loaded into the mouse naris using a cannula inserted to 9–10 mm depth. The dye was taken up by OSNs and, after a delay of 2–3 d, transported to their terminals in the glomerulus[40].

***In vivo* imaging.** 2- to 3-month-old *Cx30-CreERT2*; *R26-lsl-GCaMP3* mice, nose-loaded with CaRuby-Nano, were anesthetized with an intraperitoneal injection of ketamine (100 mg kg^{-1}) and xylazine (8 mg kg^{-1}) in 0.9% NaCl, then head-fixed to a stereotactic frame. Body temperature was monitored using a rectal probe and maintained at 36–37 °C using a heating pad (FHC). An incision was made at the base of the skull, and the cisterna magna was opened and drained of CSF. A craniotomy was drilled over the dorsal olfactory bulb, and the dura was removed. The brain was then stabilized with 2% (w/v) agarose. Anesthesia was assessed by the lack of a toe-pinch response and breathing rate (>2 Hz) monitored by a pneumogram transducer (Biopac Systems). To image RBC velocity, Texas Red dextran (70 kDa) was administered intravenously by either retro-orbital or tail vein injection. A low concentration (50-µl bolus of 30 µM in 0.9% NaCl) was used to allow for the simultaneous imaging of the relatively faint astrocytic Ca^{2+} signals. After loading, RBCs could be detected in capillaries as dark shadows against the fluorescently labeled plasma, and a line scan along the axis of the capillary was used to infer RBC velocity[49]. Capillaries were defined as having a luminal diameter of <6 µm.

Following surgery, mice were transferred to a custom-built two-photon microscope, and the bulb was imaged using a 40× water-immersion objective (Olympus). Fluorophores were excited at 910 nm. GCaMP3 fluorescence (K_d 660 nM, em 510 nm) was collected using a 570-nm short-pass filter. Texas Red (em 615 nm) and CaRuby-Nano (K_d of 44 180 nM, em 610 nm) fluorescence were collected on the same PMT using a HQ 620/40 nm bandpass filter (Chroma). Pixel dwell time was fixed at 6.2 µs. Spatial resolution was improved by increasing the number of pixels per micron, up to a maximum of 2. The maximum frame rate used in the study was 25 Hz.

Odors (amyl acetate or ethyl valerate) were presented for 3 s in humidified air (1 l min^{-1}) supplemented with 30% O_2 using a custom-built olfactometer[40].

doi:10.1038/nn.3906

To measure OSN and astrocyte Ca^{2+} responses alone, a movie of the ROI covering the entire glomerulus was recorded. To measure RBC velocity simultaneously, a broken line scan along a glomerular capillary and through the neighboring glomerular neuropil was used[50].

Data analyses. *Acute slices.* The analysis was performed with Igor Pro 6.0 (WaveMetrics), pClamp 9 (Molecular Devices) and custom-made software (LabVIEW). Fluorescence signals were analyzed in ROIs covering the entire somata of astrocytes and neurons. Normalized changes in Rhod-2 fluorescence were calculated as $\Delta F/F = (F - F_0) / F_0$, i.e., the difference between Rhod-2 signal (F) and baseline Rhod-2 fluorescence (F_0) calculated as an average of 5–10 s before stimulus onset, divided by F_0. To compare F_0 changes between control conditions (F_0_control), in the presence of TBOA/TFB-TBOA (F_0_TBOA) and after washout (F_0_washout), the normalized ΔF_0 changes were calculated as (F_0_TBOA (or F_0_washout) – F_0_control) / F_0_control. The peaks of Rhod-2 signals were determined from a five-point box-filtered trace that was obtained after averaging raw traces. The threshold for measuring the onset of OSN-evoked Ca^{2+} transients was set where the change in F relative to F_0 was greater than 2 × s.d. of the baseline signal for at least 0.5 s (more than 3 frames). Latencies of the evoked Ca^{2+} transients were calculated from the stimulus onset. Ca^{2+} signals induced by puff application were analyzed first by averaging the Ca^{2+} responses to multiple trials. The response was then calculated as an integral of the $\Delta F/F$ during the Ca^{2+} response (10–30 s after the beginning of the puff application) divided by the duration to give a mean $\Delta F/F$ during the response period.

For statistical analyses, we used the Wilcoxon signed-rank test except for **Figure 4d**, where a two-tailed paired t-test was used. In this case, astrocyte responses to OSN stimulation (all control condition $n = 18$) were normally distributed according to a Kolmogorov-Smirnov test. For all tests, the significance threshold was $P < 0.05$; *exact P* values are not presented when $P < 0.001$. All data are presented as mean ± s.e.m. No statistical methods were used to predetermine sample sizes. Data collection and analysis were not performed blinded to the conditions of the experiments. There was no randomization of data collection or processing.

In vivo. Fluorescence signals were analyzed using custom-written software (LabVIEW and MATLAB), and figures were prepared in Igor Pro 6.0 (WaveMetrics).

A **Supplementary Methods Checklist** is available.

49. Kleinfeld, D., Mitra, P.P., Helmchen, F. & Denk, W. Fluctuations and stimulus-induced changes in blood flow observed in individual capillaries in layers 2 through 4 of rat neocortex. *Proc. Natl. Acad. Sci. USA* **95**, 15741–15746 (1998).
50. Jukovskaya, N., Tiret, P., Lecoq, J. & Charpak, S. What does local functional hyperemia tell about local neuronal activation? *J. Neurosci.* **31**, 1579–1582 (2011).